JBC ARTICLE

Gluconeogenic precursor availability regulates flux through the glyoxylate shunt in *Pseudomonas aeruginosa*

Received for publication, June 19, 2018, and in revised form, July 18, 2018 Published, Papers in Press, July 20, 2018, DOI 10.1074/jbc.RA118.004514

Audrey Crousilles, Stephen K. Dolan, Paul Brear, Dimitri Y. Chirgadze, and Martin Welch[1]

From the Department of Biochemistry, University of Cambridge, Tennis Court Road, Cambridge, CB2 1QW, United Kingdom

Edited by Wolfgang Peti

The glyoxylate shunt bypasses the oxidative decarboxylation steps of the tricarboxylic acid (TCA) cycle, thereby conserving carbon skeletons for gluconeogenesis and biomass production. In *Escherichia coli*, carbon flux is redirected through the first enzyme of the glyoxylate shunt, isocitrate lyase (ICL), following phosphorylation and inactivation of the TCA cycle enzyme, isocitrate dehydrogenase (ICD), by the kinase/phosphatase, AceK. In contrast, mycobacterial species lack AceK and employ a phosphorylation-insensitive isocitrate dehydrogenase (IDH), which is allosterically activated by the product of ICL activity, glyoxylate. However, *Pseudomonas aeruginosa* expresses IDH, ICD, ICL, and AceK, raising the question of how these enzymes are regulated to ensure proper flux distribution between the competing pathways. Here, we present the structure, kinetics, and regulation of ICL, IDH, and ICD from *P. aeruginosa*. We found that flux partitioning is coordinated through reciprocal regulation of these enzymes, linking distribution of carbon flux to the availability of the key gluconeogenic precursors, oxaloacetate and pyruvate. Specifically, a greater abundance of these metabolites activated IDH and inhibited ICL, leading to increased TCA cycle flux. Regulation was also exerted through AceK-dependent phosphorylation of ICD; high levels of acetyl-CoA (which would be expected to accumulate when oxaloacetate is limiting) stimulated the kinase activity of AceK, whereas high levels of oxaloacetate stimulated its phosphatase activity. In summary, the TCA cycle–glyoxylate shunt branch point in *P. aeruginosa* has a complex enzymology that is profoundly different from those in other species characterized to date. Presumably, this reflects its predilection for consuming fatty acids, especially during infection scenarios.

The glyoxylate shunt is an anaplerotic pathway that bypasses the oxidative decarboxylation steps of the TCA[2] cycle, thereby conserving carbon skeletons for gluconeogenesis and biomass production (1). The mechanisms controlling carbon flux partitioning between the TCA cycle and glyoxylate shunt were largely worked out in the *Escherichia coli* model in the 1980s. Here, the TCA cycle enzyme, isocitrate dehydrogenase (ICD, encoded by *icd*), and the glyoxylate shunt enzyme, isocitrate lyase (ICL, encoded by *aceA*) compete for available isocitrate. ICD has a much lower K_m for isocitrate (K_m = 8 μM (2)) than ICL (K_m 604 μM (3)), so to obtain significant flux through the glyoxylate shunt, ICD needs to be inactivated. This is accomplished by reversible phosphorylation of ICD on Ser-113, mediated by a dual function kinase/phosphatase, AceK (4). Phosphoserine 113 is thought to electrostatically repulse isocitrate, thereby preventing substrate binding (5). Consequently, when the kinase activity of AceK is dominant, ICD becomes phosphorylated and inactivated, allowing carbon flux to be redirected through the glyoxylate shunt. In contrast, when the phosphatase activity of AceK dominates, flux is restored through the TCA cycle. The ratio of kinase/phosphatase activity in AceK is controlled by allosteric regulators (6).

Not all bacteria share the same enzymology as *E. coli* at the TCA cycle–glyoxylate shunt branch point (TGB); some bacteria encode a second, AceK-insensitive isocitrate dehydrogenase isozyme, IDH. Genome sequencing efforts have revealed that some species, such as the industrially important fermenter *Corynebacterium glutamicum*, contain only *idh*, whereas others contain only *icd* (*e.g. E. coli*). Generally, and as might be expected, there is a strong correlation between the presence of genes encoding ICD, ICL, and AceK in a genome. However, there are exceptions to this. For example, *Mycobacterium tuberculosis* encodes ICL, ICD, and IDH, but lacks AceK. Without a mechanism to inactivate ICD, this raises the question of how flux is redirected through the glyoxylate shunt in this organism. This was partially resolved by the finding that ICD appears to be fully dispensable for flux through the TCA cycle in *M. tuberculosis* (7), so only ICL and IDH compete for the pool of isocitrate. Recent work done in a related species of mycobacteria (*Mycobacterium smegmatis*) indicates that flux partitioning at the TGB is determined primarily by allosteric activation of IDH by ICL-derived glyoxylate (7).

An additional layer of unexplored complexity is seen in the opportunistic human pathogen *Pseudomonas aeruginosa*. Here, *three* enzymes compete for isocitrate: ICD, IDH, and ICL. Moreover, *P. aeruginosa* also encodes the ICD kinase/phosphatase, AceK. This raises the question of how AceK-mediated post-translational regulation of ICD activity is integrated with the activities of ICL and IDH. The lack of clarity here is ironic,

---

This work was supported by Biotechnology and Biological Sciences Research Council (BBSRC) Grant BB/M019411/1. The authors declare that they have no conflicts of interest with the contents of this article.

This article contains Table S1 and Figs. S1–S12.

The atomic coordinates and structure factors (codes 6G1O and 6G3U) have been deposited in the Protein Data Bank (http://wwpdb.org/).

[1] To whom correspondence should be addressed. Tel.: 44-1223-333-653; E-mail: mw240@cam.ac.uk.

[2] The abbreviations used are: TCA, tricarboxylic acid; ICD, isocitrate dehydrogenase; ICL, isocitrate lyase; IDH, isocitrate dehydrogenase; TGB, TCA cycle–glyoxylate shunt branch point; GFC, gel filtration; MALS, multiangle light scattering; AUC, analytical ultracentrifugation; PEP, phosphoenolpyruvate; PDB, Protein Data Bank; Ni-NTA, nickel-nitrilotriacetic acid; TEV, tobacco etch virus.

Table 1

Kinetic parameters of ICL, IDH, and ICD

K_m and $V_{\max}$ values were calculated after fitting to the Michaelis–Menten curve in GraphPad Prism version 6. Values of k_{cat} were derived from $V_{\max}$. NA, not applicable.

	K_m	$V_{\max}$	k_{cat}[a]	k_{cat}/K_m ($s^{-1}/\mu M$)	K_i (mM)	Comments
	μM	*ΔmM/s*	s^{-1}			
ICL						
Isocitrate	12.2	0.8	18.8	1.6	NA	Substrate
Citrate	18.8	0.8	17.7	0.9	15.8	Noncompetitive
Coenzyme A	22.6	0.6	14.9	0.7	3.9	Noncompetitive
Glycolic acid	18.2	0.5	12.2	0.7	1.8	Noncompetitive
Itaconic acid	6.3	0.4	8.7	1.4	0.9	Uncompetitive
Maleic acid	3.6	0.3	6.3	1.8	NA	Mixed
Malic acid	16.6	0.7	15.3	0.9	4.4	Noncompetitive
Malonic acid	12.0	0.5	12.2	1.0	2.9	Uncompetitive
Nitropropionic acid	6.9	0.3	7.5	1.1	1.0	Uncompetitive
Oxaloacetate	18.4	0.5	11.0	0.6	1.4	Noncompetitive
Phosphoenolpyruvate	6.0	0.4	8.9	1.5	NA	Mixed
Pyruvate	18.2	0.5	11.8	0.7	1.7	Noncompetitive
Succinate	7.8	0.3	7.1	0.9	0.9	Uncompetitive
IDH						
Isocitrate	17.7	0.5	183.7	10.4	NA	Substrate
Glyoxylate	20.7[b]	2.3	925.2	44.8	NA	Noncompetitive
Oxaloacetate	39.2[b]	3.0	1210.9	30.9	NA	Uncompetitive
Pyruvate	42.0[b]	3.5	1408.2	33.6	NA	Uncompetitive
NADP	34.5[b]	0.5	210.9	6.1	NA	Substrate
Glyoxylate	160.4[b]	3.8	1544.2	9.6	NA	Uncompetitive
Oxaloacetate	29.0[b]	3.0	1217.7	42.0	NA	Noncompetitive
Pyruvate	49.5	3.4	1381.0	27.9	NA	Noncompetitive
ICD						
Isocitrate	25.6	1.3	608.8	23.8	NA	Substrate
α-Ketoglutarate	64.0	1.6	745.8	11.7	0.666	Competitive
NADP	32.3	1.5	684.9	21.2	NA	Substrate

[a] The value of E_t was based on the most likely oligomeric status of the native protein from the combined crystallographic and solution structure data. ICL was assumed to be a tetramer, ICD a dimer, and IDH a monomer.

[b] Regulators of IDH altered the kinetics from hyperbolic to sigmoidal with respect to isocitrate, so the reported values in the table are K_{half}, instead of K_m. The value of K_i was determined differently, depending on the type of inhibition observed. In the case of competitive inhibition, we used $K_i = ((K_m \times [I])/(K_m(\text{obs}) - K_i'))$, whereas for noncompetitive inhibition, we used $K_i = [I]/((V_m/V_{m(\text{obs})}) - 1))$. For uncompetitive inhibition, K_i' was determined from the y axis intercept of the Lineweaver–Burk plot, assuming that $K_i' = [I]/(y_{\text{intercept}} \times V_{\max}) - 1))$. In all the cases, $[I] = 1$ mM.

especially given that Kornberg and Krebs originally elucidated the glyoxylate shunt in a *Pseudomonas* strain, KB1 (8).

Results

To investigate the enzymology of flux partitioning in *P. aeruginosa* TGB further, we cloned and purified ICL, ICD, IDH, and AceK from this organism. Kinetic analysis of the purified enzymes revealed that in striking contrast with *E. coli* and *M. smegmatis*, *P. aeruginosa* ICL has a *higher* affinity for isocitrate (K_m 12 μM) compared with the competing dehydrogenases, ICD (K_m 26 μM) and IDH (K_m 18 μM) (Table 1 and Fig. S1). ICD and IDH shared similar K_m values for their other substrate, NADPH (32 and 34 μM, respectively). ICD and IDH were expressed at comparable levels during growth on either glucose or acetate (Fig. S1*E*). Commensurate with earlier observations that there is significant flux through the glyoxylate shunt even during growth on glucose (9), ICL was expressed (albeit at low levels) on this substrate. However, ICL expression increased during growth on acetate. Again, this is consistent with earlier observations that acetate induces expression of the ICL-encoding gene, *aceA* (10).

Structure and regulation of P. aeruginosa ICL

At 531 amino acids, *P. aeruginosa* ICL is longer than *E. coli* ICL (434 amino acids) and shares only 27% amino acid sequence identity with the latter. It also lies on a distinct branch of the evolutionary tree for this enzyme (which also includes ICL from pathogens such as *Burkholderia cepacia* and *Acinetobacter baumanii*), with no structurally characterized homologues to date (Fig. S2). To investigate this further, we solved the X-ray crystal structure of *P. aeruginosa* ICL to 1.9 Å resolution (PDB code 6G1O), with Ca^{2+} and glyoxylate embedded in the active site (Fig. 1). Crystallographic statistics are given in Table S1.

The presence of a Ca^{2+} (which was coordinated with the glyoxylate ligand and three water molecules) in the ICL active site was confirmed using Checkmymetal. In the crystal structure, there is one ICL polypeptide per asymmetric portion of the unit cell, which belonged to the I222 space group (Fig. 1*A*). These polypeptides are related by a crystallographic 2-fold axis to yield a tetrameric structure (Fig. 1*B*) with extensive contacts made between each protomer (Fig. S3). This is consistent with gel filtration/multiangle light scattering (GFC/MALS) and analytical ultracentrifugation (AUC) data indicating that ICL behaves as a 231-kDa tetramer in solution (Fig. S4). Each protomer in *P. aeruginosa* ICL is composed of 17 α-helices and 14 β-strands arranged around a central TIM barrel-like core (secondary structure assignments are shown in Fig. S5). However, the overall fold of each protomer is distinct when compared with ICL from *E. coli* and *M. tuberculosis* (Fig. 1*C*). In particular, helices α1 and α2 of *P. aeruginosa* ICL are flipped as a unit by almost 180° relative to the axis of α3, and α6 is extended by an additional four helical turns. In addition, α13 and α14 extend away from the globular core of the protein, generating structural projections that give the tetramer a distinctly rugged, starlike profile. The most obvious difference, however, is the presence of a relatively unstructured "head-domain" spanning the region between Ile-272 and Ile-306. The head domains of adjacent protomers form some of the more intimate contacts underpinning tetramer formation (Fig. 1*B* and Fig. S3). Interestingly, ICL from the fungus *Aspergillus nidulans* also has a headlike domain, although this is rich in α-helices and does not appear to play a significant role in interprotomer interactions (11).

The catalytic core of the enzyme is conserved. The active site of ICL is composed of two distinct parts: those residues associated with the β-strands and loops around the rim of the TIM barrel and a flexible loop of structure between β4 and β5 (12). The latter contains the catalytic general base, Cys-222 (*P. aeruginosa* numbering). In our structure, this β4-β5 loop points away from the active site. Presumably, in the presence of isocitrate, this loop swings inwards to cap the active site, as it does in ICL from *M. tuberculosis* (13). The glyoxylate moiety in our structure is displaced by 6 Å toward the β4-β5 loop, leaving it poised ready to exit the active site, although it remains anchored on the enzyme through coordination with the Ca^{2+} (Fig. 1*D*).

Given its position at the TGB, it is unsurprising that the activity of *P. aeruginosa* ICL is modulated by certain metabolites. *P. aeruginosa* ICL activity was inhibited by oxaloacetate, pyruvate, succinate, phosphoenolpyruvate (PEP), and CoA (Fig. 2). No activators were identified. Oxaloacetate (K_i = 1.9 mM), pyruvate (K_i = 2 mM), and CoA (K_i = 1.2 mM) all inhibited the

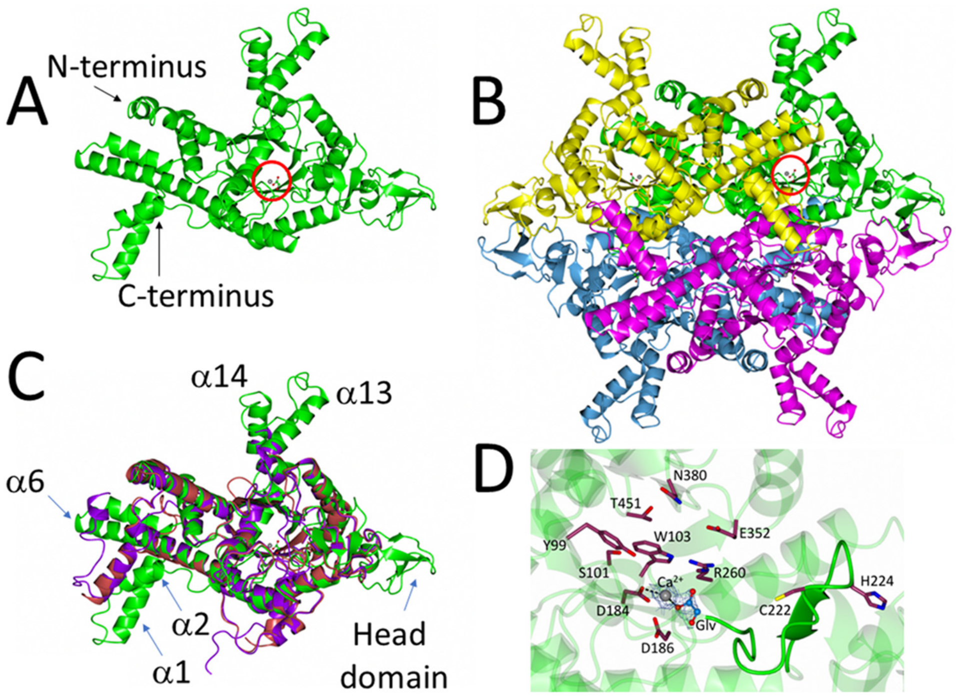

Figure 1. Structure of *P. aeruginosa* ICL. *A*, *cartoon representation* of a single isocitrate lyase protomer from *P. aeruginosa* (PDB code 6G1O). The bound Ca^{2+} and glyoxylate are indicated with a *red circle*. *B*, quaternary structure of the isocitrate lyase in the crystal. Note the β strand–rich head domains on either side of the tetramer and the α-helical projections (α13 and α14 in each protomer) *above* and *below* the structure. The Ca^{2+} and glyoxylate in one of the protomers are *circled*. *C*, superposition of *P. aeruginosa* ICL (*green*), *M. tuberculosis* ICL (*purple*; PDB code 1F8I), and *E. coli* ICL (*red*; PDB code 1IGW), revealing that the catalytic core of the enzyme is highly conserved. Consistent with this, the root mean square deviation between *P. aeruginosa* and *E. coli* ICL is 1.35 Å, and the root mean square deviation between *P. aeruginosa* and *M. tuberculosis* ICL is 1.30 Å. However, note how α1 and α2 are flipped by 180° in *P. aeruginosa* ICL, the extended helices α13 and α14, and the presence of a head domain (absent from *M. tuberculosis* and *E. coli* ICL. *D*, conserved active site residues in *P. aeruginosa* ICL. The β4-β5 loop containing the general base, Cys-222, is *highlighted*. The electron density map for glyoxylate and Ca^{2+} is *contoured* at 1.7σ.

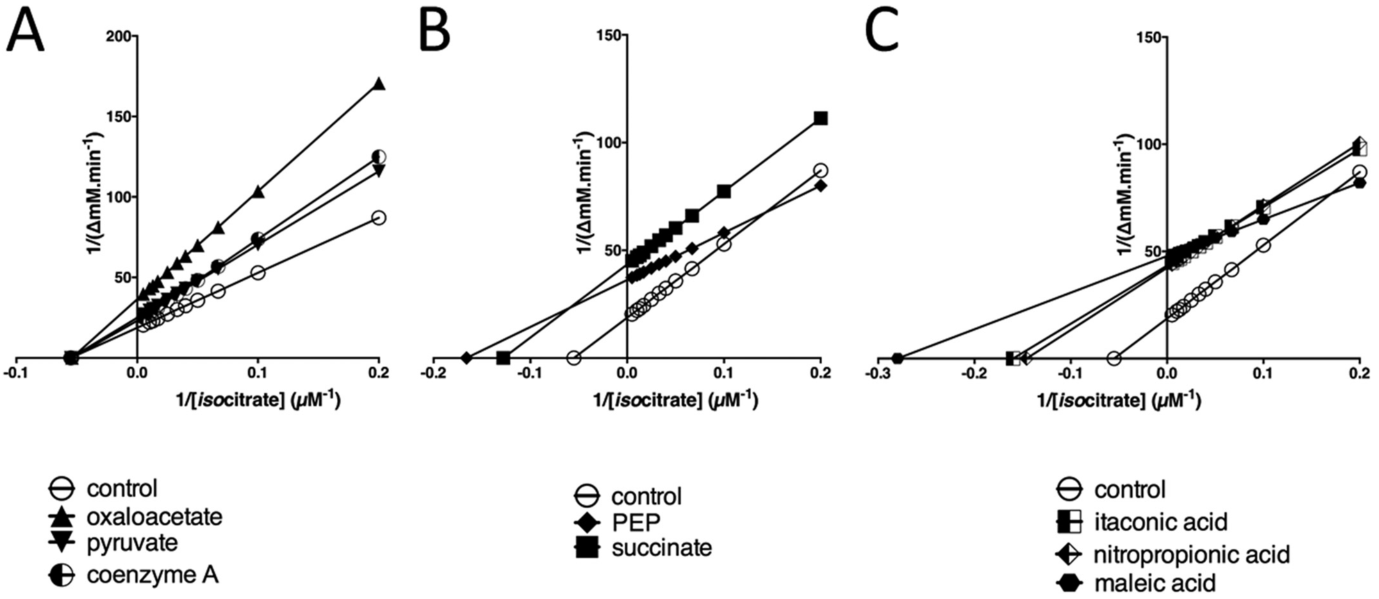

Figure 2. Inhibition of *P. aeruginosa* ICL activity by small molecules. *A*, CoA, oxaloacetate and pyruvate noncompetitively inhibit ICL. Shown is a Lineweaver–Burk transformation of ICL kinetic data obtained in the presence of no addition (control) or in the presence of oxaloacetate, pyruvate, or CoA. *B*, Lineweaver–Burk plot showing that succinate inhibits ICL uncompetitively, whereas phosphoenolpyruvate displays mixed inhibition. *C*, itaconate and nitropropionate inhibit ICL uncompetitively, whereas maleic acid displays mixed inhibition. The plots were generated using GraphPad Prism version 6. All small molecules (except the substrate) were added at 1 mM final concentration.

enzyme noncompetitively (Fig. 2*A*), whereas the reaction product, succinate, inhibited uncompetitively ($K_i' = 0.6$ mM) and PEP displayed mixed inhibition (Fig. 2*B*). In common with other isocitrate lyases, the enzyme was also susceptible to uncompetitive inhibition by itaconic acid ($K_i' = 0.5$ mM) and nitropropionic acid ($K_i' = 0.6$ mM) (14, 15) and potent mixed inhibition by maleic acid (Fig. 2*C*). The latter may reflect the partial structural similarity between PEP and maleic acid.

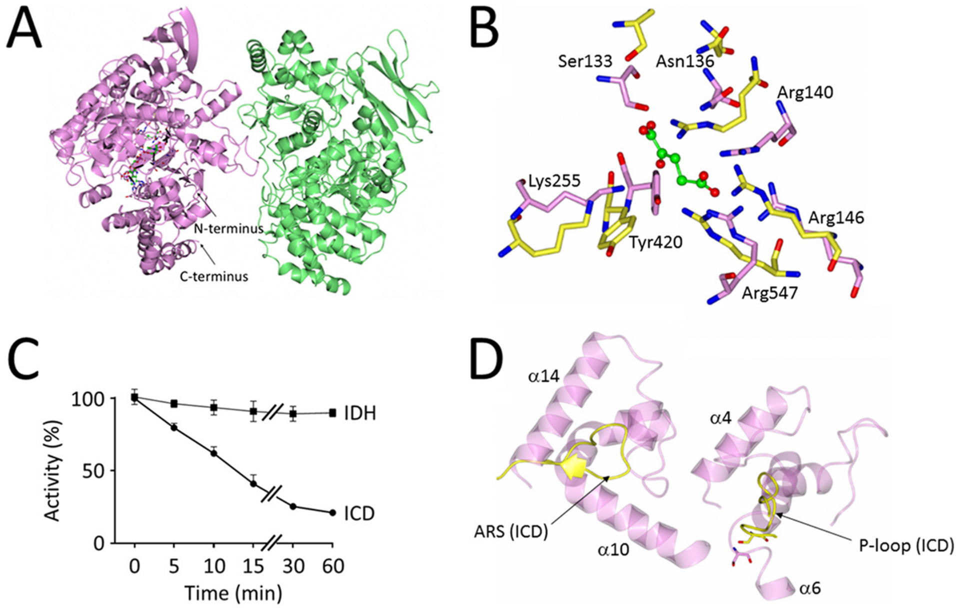

Figure 3. Structure and regulation of *P. aeruginosa* IDH. *A*, *cartoon schematic* of IDH from *P. aeruginosa*. Chain A (*mauve*) contains one molecule each of NADP$^+$ and α-ketoglutarate bound in its active site. Chain B (*light green*) does not contain any bound small molecules. The two IDH chains in the asymmetric unit do not show enough interprotein contacts to warrant being labeled as protomers in a dimer. *B*, *close-up view* of the conserved active site residues in *P. aeruginosa* IDH (*light pink*, PDB code 6G3U) and *P. aeruginosa* ICD (*yellow*, PDB code 5M2E). Residue numbering is based on the IDH sequence. *C*, *P. aeruginosa* ICD, but not IDH, is inactivated by AceK-dependent phosphorylation. Shown is the loss of isocitrate dehydrogenase activity over time following treatment with AceK/ATP. Reaction mixtures (200 μl) contained 100 mM Tris-HCl (pH 7.0), 1 mM ATP, 2 mM MgCl$_2$, 5 μg of purified *P. aeruginosa* AceK, and 10 μg of *P. aeruginosa* ICD or IDH (as indicated). Reactions were allowed to proceed at 37 °C, and at the indicated times, aliquots were withdrawn and assayed immediately for isocitrate dehydrogenase activity, as described under "Experimental procedures." Activity was considered to be 100% at T_0. *D*, the architecture of the active site is different in ICD and IDH. Despite the conserved constellation of active site residues (*B*) in *P. aeruginosa* ICD and IDH, the P-loop containing the phosphoserine in ICD (*yellow*) and the AceK recognition segment (*ARS*) are replaced in IDH by two helices, α10–α14 and α4–α6, respectively. This altered arrangement presumably prevents AceK from accessing the active site serine in IDH.

Structure and regulation of P. aeruginosa IDH

In *P. aeruginosa*, two isocitrate dehydrogenases, IDH and ICD, compete with ICL for isocitrate. In solution, IDH (monomeric molecular mass 82 kDa) had an apparent molecular mass of 235 kDa (GFC/MALS) or 273 kDa (AUC), suggesting that it adopts a higher-order structure (Fig. S6). To investigate the enzyme further, we solved its X-ray crystal structure (PDB code 6G3U) to 2.7 Å resolution (Fig. 3).

The asymmetric unit comprised two molecules of IDH; one (designated chain A) contained bound α-ketoglutarate and NADP, and the other (chain B) contained no bound substrate/product (Fig. 3*A*). However, the interface between these monomers was small, and analysis using PISA (16) suggested that the two molecules cannot be considered to be protomers of a functional dimer. Comparison of the three-dimensional structure of the *P. aeruginosa* A and B chains revealed large conformational differences, especially in the smaller domain of each chain (Fig. S7), suggesting that catalysis is accompanied by structural rearrangements.

The α-ketoglutarate binding cleft is sandwiched between the two IDH domains (Fig. S7*A*), with side chains from both domains involved in binding. The active site residues are remarkably well conserved between IDH and ICD (Fig. 3*B*). This is consistent with the proposed common evolutionary origins of both proteins (17) and raises the question of why IDH is not a substrate for AceK (Fig. 3*C*). Comparison of the *P. aeruginosa* IDH active site architecture with that of ICD in the AceK–ICD complex from *E. coli* (PDB code 3LCB) reveals that despite the conserved constellation of catalytic residues, the active sites are differently structured, with the two ICD motifs known to be critical for recognition by AceK (the P-loop and AceK recognition segment (*ARS*)) absent in IDH (Fig. 3*D*).

Glyoxylate was recently reported to be the principal regulator of IDH in *M. smegmatis*, enabling "rheostatic" control of flux through the glyoxylate shunt (7). However, and although glyoxylate did stimulate *P. aeruginosa* IDH activity, pyruvate and oxaloacetate were far more potent regulators. All three compounds changed the isocitrate dependence of IDH kinetics from hyperbolic to sigmoidal (Fig. 4*A*), and all had a pronounced effect on k_{cat} with only a small impact on K_m (Table 1), indicating that the enzyme is of the rarer V-type allosteric class. The shift to sigmoidal isocitrate kinetics in the presence of these activators suggests cooperativity in substrate binding, consistent with IDH adopting a higher-order structure in solution. However, these effectors had much less impact on the NADP dependence of IDH kinetics, which remained essentially hyperbolic (Fig. 4*B*). In common with previously characterized isocitrate dehydrogenases, IDH (and also ICD) was strongly inhibited by mixtures containing oxaloacetate and glyoxylate, presumably due to the nonenzymatic formation of oxalomalate (18).

Structure and regulation of ICD

The second isocitrate dehydrogenase encoded by *P. aeruginosa* is ICD. *P. aeruginosa* ICD crystallized as a dimer (Fig. 5*A* and Table S1) and also behaved as a dimer in solution (Fig. S9). The structure (PDB code 5M2E), solved to 2.7 Å resolution, was very similar to that reported for the *E. coli* enzyme (Fig. S8*A*), with a clasplike structure mediating the dimerization (19). The

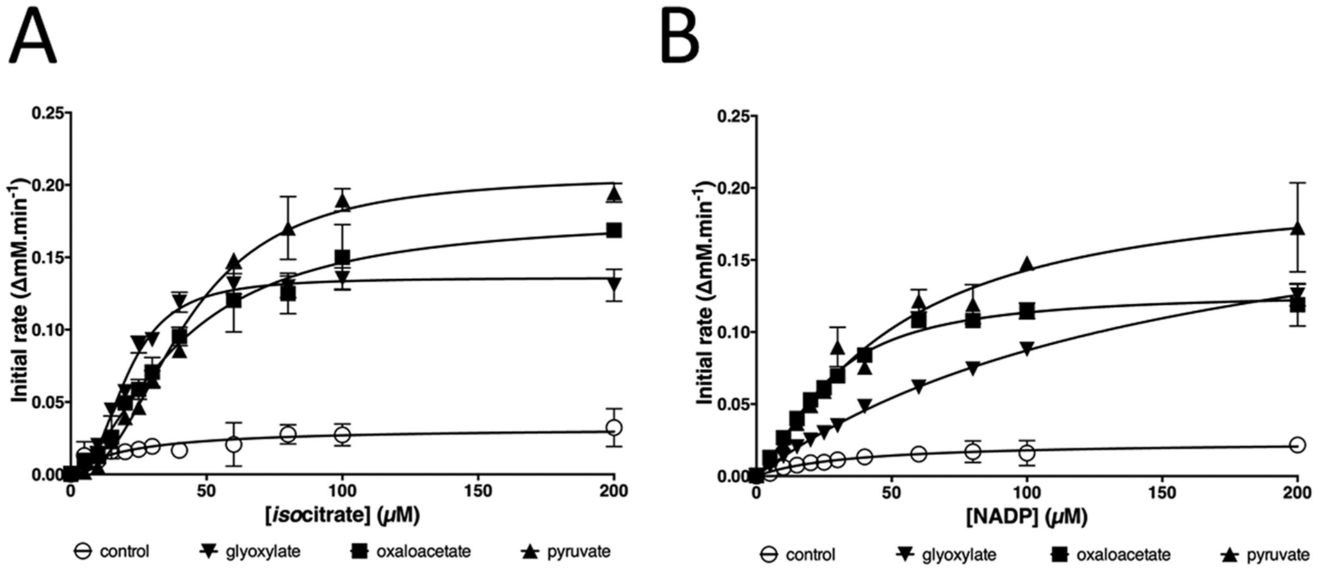

Figure 4. Pyruvate, oxaloacetate, and glyoxylate strongly activate the isocitrate dehydrogenase activity of IDH. *A*, effect of pyruvate, oxaloacetate, and glyoxylate on the isocitrate dependence of IDH kinetics. *B*, effect of pyruvate, oxaloacetate, and glyoxylate on the NADP$^+$ dependence of IDH kinetics. Each regulator was added at a 1 mM final concentration. *Error bars*, ± 1 S.D. from $n = 3$ replicates.

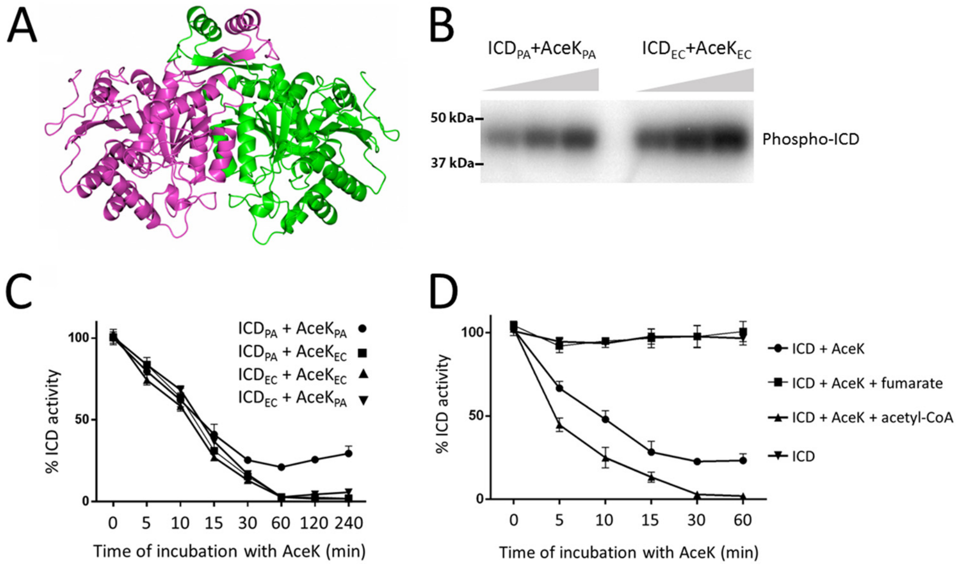

Figure 5. Regulation of *P. aeruginosa* ICD activity by AceK-dependent phosphorylation. *A*, *ribbon representation* of the ICD dimer. The two protomers are *highlighted* in *light purple* and *green*. Dimerization is largely mediated by the clasp domain, shown here at the *top* of the structure, although additional contacts between helices at the core of the structure also play a role. *B*, AceK-mediated phosphotransfer from [γ-^{32}P]ATP to ICD. Phosphotransfer was measured between *P. aeruginosa* AceK and *P. aeruginosa* ICD (AceK$_{PA}$ and ICD$_{PA}$) or between *E. coli* AceK and *E. coli* ICD (AceK$_{EC}$ and ICD$_{EC}$), as indicated. Aliquots were removed for sampling after 1-, 2-, and 3-min incubation and resolved by SDS-PAGE. Radioactivity was monitored using a PhosphorImager. *C*, *P. aeruginosa* AceK is intrinsically less efficient at phosphorylating *P. aeruginosa* ICD than *E. coli* AceK. The figure shows a "mix and match" experiment in which the efficiencies of *P. aeruginosa* and *E. coli* AceK at inactivating the ICD homologues from each species are measured. ICD$_{PA}$ and ICD$_{EC}$ can each be phosphorylated by either AceK$_{PA}$ or AceK$_{EC}$. However, the ICD$_{PA}$/AceK$_{PA}$ pair never achieves full inactivation, despite the fact that AceK$_{PA}$ fully inactivates ICD$_{EC}$ (indicating that the kinase is competent to do this) and that AceK$_{EC}$ fully inactivates ICD$_{PA}$ (indicating that the ICD is potentially fully inactivatable). Reaction conditions were as in Fig. 3. *D*, fumarate stimulates the phosphatase activity of AceK$_{PA}$ (thereby reactivating ICD), whereas acetyl-CoA stimulates the kinase activity of AceK$_{PA}$ (thereby inactivating ICD). Fumarate and acetyl-CoA were present at 5 mM concentration.

residues lining the substrate binding site were also conserved between the *E. coli* and *P. aeruginosa* enzymes (Fig. S8*B*). ICD was competitively inhibited by the reaction product, α-ketoglutarate (K_i = 666 μM; Fig. S8*C*). However, the main mode of regulation was through AceK-dependent phosphorylation (Fig. 5*B*). Interestingly, in all of our experiments with AceK and ICD from *P. aeruginosa* (hereafter, AceK$_{PA}$ and ICD$_{PA}$), the maximal inhibition attributable to AceK-mediated phosphorylation was only around 75% (Fig. 5*C*). This is not due to a lower intrinsic activity of AceK$_{PA}$, because AceK$_{PA}$ was able to completely inactivate ICD from *E. coli* (ICD$_{EC}$) (Fig. 5*C*). Comparison of the ICD$_{PA}$ and ICD$_{EC}$ active site region revealed slight differences in the spatial disposition of the P-loop required for AceK recognition (Fig. S8*D*), making it formally possible that ICD$_{PA}$ is less sensitive to AceK-mediated phosphorylation. However, AceK$_{EC}$ was able to completely inactivate ICD$_{PA}$, indicating that these local differences in P-loop conformation are unlikely to be functionally significant (Fig. 5*C*). Taken together, these data suggest that in the absence of external factors to stimulate its kinase activity, AceK$_{PA}$ cannot fully inhibit ICD$_{PA}$.

Although the *P. aeruginosa* and *E. coli* ICD enzymes are 79% identical at the amino acid sequence level, and the site of phosphorylation (Ser-115 in *P. aeruginosa* ICD) is conserved, the corresponding AceK orthologues show substantial differences. In particular, the N-terminal regulatory domain is just 35% identical between the two species. In contrast, the C-terminal catalytic domain is 60% identical and retains all of the sequence motifs thought to be important for kinase and phosphatase activity. These data suggest that *P. aeruginosa* AceK is likely to be regulated differently compared with the *E. coli* orthologue. To investigate this further, we examined how a panel of potential regulators affected AceK$_{PA}$-dependent inactivation of ICD$_{PA}$ (Fig. S10). ICD was first phosphorylated by AceK for 60 min (enough to maximally inactivate the dehydrogenase (Fig. 5*C*)). Following this, the indicated potential regulators were added, and restoration of isocitrate dehydrogenase activity was monitored after 30 min (Fig. S10*A*). As a control, and to confirm the species specificity of each regulator, we also examined (i) whether the same compounds affected AceK$_{EC}$-dependent restoration of ICD$_{EC}$ activity (Fig. S10*B*) and (ii) whether the regulators had any intrinsic impact on ICD activity (Fig. S11). With the exception of citrate (which presumably competitively blocks the ICD active site) and, to a lesser extent, glyceraldehyde 3-phosphate and phosphoenolpyruvate, none of the tested potential regulators affected ICD activity directly. The phosphatase activity of AceK$_{EC}$ was stimulated by α-ketoglutarate, glyceraldehyde 3-phosphate, 2-keto-3-deoxyphosphogluconate, pyruvate, and oxaloacetate and, to a much lesser extent, by fumarate, AMP, and ADP (Fig. S10B). The phosphatase activity of AceK$_{PA}$ was stimulated by an overlapping but larger number of regulators, including α-ketoglutarate, fructose 1,6-bisphosphate, glyceraldehyde 3-phosphate, glyoxylate, AMP, ADP, glycolate, pyruvate, and oxaloacetate. Intriguingly, fumarate was the most potent activator of the phosphatase in AceK$_{PA}$, yet this compound only weakly stimulated the phosphatase activity of AceK$_{EC}$. Similarly, succinate had no apparent effect on AceK$_{EC}$ but strongly stimulated AceK$_{PA}$ phosphatase activity. In contrast, the Entner–Doudoroff pathway intermediate, 2-keto-3-deoxyphosphogluconate, only marginally stimulated AceK$_{PA}$ phosphatase activity, yet this compound was one of the more potent activators of the AceK$_{EC}$ phosphatase. Perhaps the most noticeable regulator was acetyl-CoA. This compound weakly stimulated the phosphatase activity of AceK$_{EC}$, whereas in AceK$_{PA}$, it appeared to stimulate the kinase activity. To investigate this further, we conducted a time-course analysis of ICD$_{PA}$ activity following AceK$_{PA}$ treatment in the presence of acetyl-CoA and fumarate (Fig. 5*D*). What is immediately apparent is that, whereas fumarate maximally stimulates AceK$_{PA}$ phosphatase activity, acetyl-CoA maximally activates the AceK kinase activity, allowing the enzyme to inactivate $>$75% of the ICD, and at a faster rate than AceK alone.

Discussion

The driver behind this work is that *P. aeruginosa* exhibits a particular predilection for catabolizing fatty acids, especially during infection scenarios (20). Under these conditions, the glyoxylate shunt becomes centrally important for growth. Indeed, a mutant of *P. aeruginosa* in which ICL and malate synthase (21) are absent is cleared from a mouse pulmonary infection model within 48 h (22), indicating that the shunt is an excellent target for the development of adjuvant interventions. The physiological importance of the shunt in infection may not solely be due to the metabolic defect either; *aceA* mutants also show pronounced defects in virulence (23–25). Consequently, therapeutic agents that inhibit flux through the glyoxylate shunt (or redirect flux away from the shunt) could potentially deliver a powerful "double whammy" by eliciting both metabolic insufficiency and reduced virulence. However, a better understanding of the enzymology of the *P. aeruginosa* TGB will be essential if we are to realize its full potential as a therapeutic target. Indeed, in the current work, we show that this understanding cannot be gleaned by extrapolation from previously characterized species. For example, in *P. aeruginosa*, three enzymes compete for isocitrate, and ICL has a *higher* affinity for the substrate than the competing dehydrogenases. Also, the enzymology appears to be more complex in *P. aeruginosa* compared with other species, involving both AceK (absent in, for example, *M. smegmatis* and *M. tuberculosis*) and IDH (absent in many enterics, such as *E. coli*).

A comparison of the regulatory mechanisms established for *M. smegmatis*, *E. coli*, and *P. aeruginosa* is shown in Fig. 6. The principal regulatory mechanism associated with flux partitioning at the TGB in *M. smegmatis* is the "rheostatic control" exerted by one of the products of ICL activity, glyoxylate (7). This general mechanism appears to be conserved in *P. aeruginosa* too, although in regulatory terms, it is likely to be more nuanced. This is because not only does glyoxylate activate IDH; succinate (the other product of ICL activity) is an uncompetitive inhibitor of ICL and also a potent activator of AceK phosphatase activity (*i.e.* stimulating ICD activity). The "rheostat" in *P. aeruginosa* therefore operates at several levels. In contrast, the principal regulatory mechanism employed by *E. coli* is AceK-mediated phosphorylation/dephosphorylation of ICD. However, the mechanistic details are not the same in *E. coli* and *P. aeruginosa*. Not only is the suite of allosteric AceK regulators different in each species (presumably reflecting their distinct metabolic requirements), but so too is the extent to which AceK can intrinsically inactivate ICD. In the absence of external effectors, *P. aeruginosa* AceK can only maximally inactivate around 75–80% of the ICD present, and it is still not clear (from a mechanistic viewpoint) how the system "titrates" relative ICD inhibition. Overall, our data indicate that the control of flux through the TGB in *P. aeruginosa* is far more finely balanced than it is in the mycobacteria or the enterics. Also, the most potent TGB regulators in *P. aeruginosa* are gluconeogenic precursors. These compounds feature relatively little in the control mechanisms reported for other organisms characterized to date.

The key regulators in the *P. aeruginosa* system are oxaloacetate and pyruvate, which reciprocally regulate ICL and IDH, thereby elegantly coordinating metabolic flux partitioning between the TCA cycle and glyoxylate shunt (a more comprehensive schematic of the regulatory interactions identified in

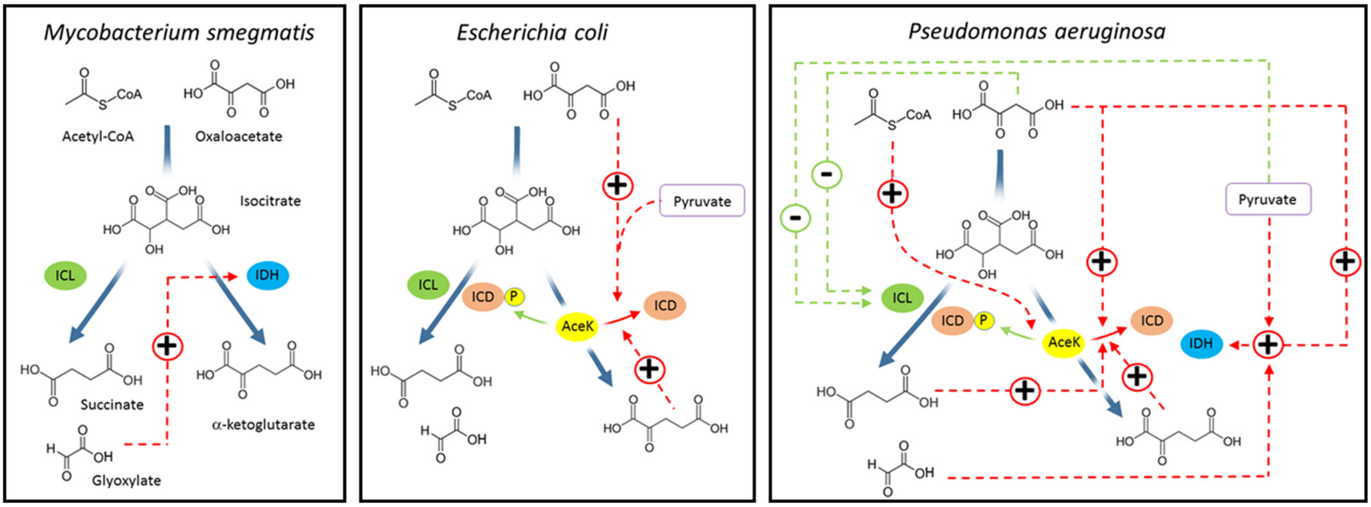

Figure 6. Comparison of TGB regulatory mechanisms in *M. smegmatis*, *E. coli*, and *P. aeruginosa*. Interactions that stimulate the target enzyme are shown in *red*, whereas interactions that inhibit the target enzyme are shown in *green*. For simplicity, we have only shown the regulatory interactions of the molecules depicted in the figure. A more comprehensive schematic of the regulatory interactions established for *P. aeruginosa* is shown in Fig. S12. Note that for simplicity, the pathway from acetyl-CoA and oxaloacetate to isocitrate is depicted as a single step in the figure, whereas this conversion is catalyzed by the sequential action of citrate synthase and aconitase in the cell.

the current study is shown in Fig. S12). When these compounds are abundant (signaling to the cell that there are sufficient gluconeogenic precursors for biomass production), IDH becomes activated and ICL inhibited, leading to greater flux around the TCA cycle (Fig. S12*A*). In a similar vein, oxaloacetate and pyruvate also stimulate the phosphatase activity of AceK, leading to increased ICD activity. In contrast, when these gluconeogenic precursors are in short supply, IDH becomes deactivated, and ICL becomes disinhibited, thereby restoring flux through the glyoxylate shunt (Fig. S12*B*). It is worth noting that ICD activity also becomes depressed via a different mechanism when demand for gluconeogenesis is high. Acetyl-CoA strongly stimulates the kinase activity of AceK, leading to inactivation of ICD (again, promoting flux through the glyoxylate shunt). This is significant because acetyl-CoA would be expected to accumulate during growth on fatty acids or acetate or when its condensation partner in the TCA cycle, oxaloacetate, is in short supply (signaling that anaplerosis is necessary). As might be expected, uncharged CoA was an inhibitor of ICL, suggesting that flux through the bifurcation point is also partially dictated by enzymatic surveillance of the acetyl-CoA/CoA ratio. As outlined above, we also found that the products of ICL activity *per se* play an important role in coordinating flux partitioning, although in *P. aeruginosa*, this appears to be secondary compared with the more dominant role(s) played by oxaloacetate, pyruvate, and acetyl-CoA.

Unlike most other organisms characterized to date, the ICL in *P. aeruginosa* has a lower K_m for isocitrate than the isocitrate dehydrogenases. The low K_m of ICL for isocitrate means that flux through the isocitrate dehydrogenases does not need to be greatly decreased to obtain flux through the glyoxylate shunt. Given the ecology of *P. aeruginosa*, this may be important, especially when demand for NADPH is high (*e.g.* during oxidative stress or anabolism). The isocitrate dehydrogenase reaction is one of the main sources of NADPH in the cell (26), and it may be that *P. aeruginosa* has evolved a "belt-and-braces" solution to ensure that it never runs out of this important antioxidant, even when the demand for flux through the glyoxylate shunt is high. This may also explain why it encodes two independently (albeit similarly) regulated isocitrate dehydrogenases, ICD and IDH. The same logic may also explain why, even after prolonged exposure to AceK, ICD retains some activity (although this was not the case in *E. coli*, where 100% inhibition was achieved after treatment with either AceK_{PA} or AceK_{EC}). Complete ICD_{PA} inhibition was only observed in the presence of acetyl-CoA, presumably because an accumulation of this metabolite indicates to the cell that the "relief valve" of the glyoxylate shunt needs to be fully opened.

Although ICD and IDH were expressed at similar levels during growth on glucose and acetate, ICL showed strong induction on the latter. Presumably, this reflects induction of the *aceA* gene, and this has been noted by earlier workers (10). However, and unlike the situation in *E. coli*, *aceA* is expressed at appreciable levels on glucose, and there is significant flux through the glyoxylate shunt on this carbon source (27). This may reflect the fact that under some conditions, optimal virulence depends upon flux through the glyoxylate shunt (23). We do not currently know why this is. However, given that bacterial virulence is a trait that is ultimately geared toward nutrient acquisition, it is hardly surprising that virulence and central metabolism should be integrally linked. Furthermore, and because flux partitioning through the TGB is a convenient indicator of anabolic *versus* catabolic demand in the cell, the evolutionary association of this particular metabolic "node" with virulence seems reasonable. The roughly comparable affinities of IDH, ICL, and ICD for their common substrate, isocitrate, coupled with the reciprocal regulation of flux through the glyoxylate shunt and TCA cycle in *P. aeruginosa* (demonstrated in this work) and the large dynamic range of *aceA* gene expression, are likely to lead to a more graded metabolic response than the ultrasensitive response associated with the TGB in *E. coli* (for example). This, in turn, would allow *P. aeruginosa* to tune its virulence in a more incremental fashion to the specific challenges encountered during infection scenarios.

One of the more remarkable observations made in this work relates to the structure of ICL. This large protein is an established drug target (28) and clearly responds to multiple regulators. We found that much of the significant additional sequence present in this subclass of ICL enzymes manifests itself as structural features projecting away from the globular core of the enzyme. Although we do not yet know what these projections do, one possibility (given their surface exposure) is that they are involved in protein–protein interactions, and we are currently investigating this. Another area of ongoing interest is to understand at an atomic level of resolution how the regulator molecules exert their effects, especially on ICL and IDH. V-type allosteric regulators remain relatively poorly characterized, and a better understanding of these may open the way toward the design of drug-like "anti-activators" as well as inhibitors.

In conclusion, we have shown that the TGB in *P. aeruginosa* has a complex enzymology that is profoundly different from that in all other organisms for which the TGB has been characterized to date. This notwithstanding, common themes are discernable among the identified regulatory molecules, and the structural data lay a solid groundwork for downstream drug design efforts.

Experimental procedures

Cloning, overexpression, and purification

The ORFs encoding the ICL (PA2634), IDH (PA2624), and ICD (PA2623) enzymes were PCR-amplified from the genomic DNA of *P. aeruginosa* strain PAO1 and cloned into a derivative of the NEB vector pMAL-c2X, which had been previously modified to introduce a hexahistidine tag onto the N terminus of the maltose-binding protein. The constructs were confirmed by DNA sequencing and introduced into *E. coli* DH5α. For overexpression, the cultures were grown with good aeration in LB medium at 37 °C to $A_{600} = 0.6$. Isopropyl 1-thio-β-D-galactopyranoside was then added to a final concentration of 0.3 mM, and growth was allowed to continue for a further 2 h. The cells were harvested by sedimentation (3430 × *g*, 20 min, 4 °C), and the pellets were resuspended in 60 ml of buffer A (200 mM NaCl, 20 mM Tris-HCl, 1 mM EDTA, 1 mM DTT, pH 7.4) containing a Complete EDTA-free protease inhibitor mixture tablet (Roche Applied Science). The cells were lysed by sonication on ice, and the cell debris was removed by sedimentation (15,000 × *g*, 30 min, 4 °C). The supernatant was applied to an amylose resin column and washed (overnight) with 500 ml of buffer A at 4 °C. The protein was then eluded in 10 ml of buffer B (200 mM NaCl, 20 mM Tris-HCl, 1 mM EDTA, 10 mM maltose, pH 7.4). The eluted sample was dialyzed against 2 × 1 liter of buffer C (50 mM NaCl, 25 mM Tris-HCl, 10% (v/v) glycerol, pH 7.4). Following this, the sample was concentrated and cleaved with Factor Xa protease (1:100 ratio of protease/sample) at 6 °C for 24 h with constant gentle mixing. The protease was removed using *p*-aminobenzamidine–agarose, and the cleaved protein mixture was applied to a column (2-ml packed resin volume) of Ni-NTA resin equilibrated with buffer D (100 mM NaCl, 50 mM Tris-HCl, 5% (v/v) glycerol, 5 mM β-mercaptoethanol, pH 7.5) to remove the His$_6$-maltose-binding protein tag. The flow-through (consisting of cleaved purified target protein) was collected and dialyzed against buffer E (100 mM NaCl, 25 mM Tris-HCl, 10% (v/v) glycerol, 1 mM EDTA, 1 mM DTT, pH 7.5). The dialyzed sample was concentrated by ultrafiltration and then snap-frozen in liquid nitrogen for storage at −80 °C. Protein concentration was determined spectrophotometrically using the calculated molar extinction ($\epsilon_{\text{calc}} = 54{,}320\ \text{M}^{-1}\cdot\text{cm}^{-1}$ (ICL), $82{,}280\ \text{M}^{-1}\cdot\text{cm}^{-1}$ (IDH), and $57{,}870\ \text{M}^{-1}\cdot\text{cm}^{-1}$ (ICD)).

The AceK (PA1376), ICD$_{\text{PA}}$, and ICD$_{\text{EC}}$ (from *E. coli* strain DH5α) used for phosphotransfer/AceK inhibition assays were purified slightly differently. The PCR-amplified ORFs were cloned into the expression vector pET-19m, which introduces a TEV-cleavable N-terminal hexahistidine tag onto each protein. For purification of the His$_6$-tagged proteins, the cells were grown in LB medium at 37 °C with good aeration to $A_{600} = 0.5$. The temperature was then lowered to 20 °C, and isopropyl 1-thio-β-D-galactopyranoside was added to a 0.5 mM final concentration to induce expression of the cloned genes. The induced cultures were grown for a further 16 h and then harvested by sedimentation (6000 × *g*, 4 °C, 15 min). The cell pellet was resuspended in 20 ml of buffer F (50 mM sodium phosphate, 200 mM NaCl, 10% (v/v) glycerol, pH 8.0), and the cells were ruptured by sonication (3 × 10 s, Soniprep 150, maximum power output). The cell lysate was clarified by centrifugation (11,000 × *g*, 4 °C, 30 min), and the supernatant was filtered through a 0.45-μm filter. The filtered lysate was then loaded onto an Ni-NTA column (2-ml packed resin bed volume), and the column was washed overnight at 4 °C with buffer F containing 10 mM imidazole. The His$_6$-tagged proteins were eluted with buffer F containing 250 mM imidazole. The purified protein was mixed with His$_6$-tagged TEV-protease and dialyzed overnight at 4 °C against 2 liters of buffer G (20 mM Tris-HCl, 50 mM NaCl, 5% (v/v) glycerol, pH 7.5). The proteins thus released were cleaned up by batch extraction in a slurry of Ni-NTA resin equilibrated in buffer G. AceK$_{\text{EC}}$ was expressed and purified as above, but from a modified pET-15b vector (a generous gift from Prof. Z. Jia) (29).

Gel filtration and AUC

GFC—Analytical gel filtration with multiangle light scattering was carried out using a 300 × 7.8-mm TSK-Gel G3000 SWXL column (Toso Haas) equilibrated with 150 mM NaCl, 20 mM Tris-HCl (pH 8.0) operating at a flow rate of 0.5 ml min^{-1}. The column eluate was monitored in-line with a Mini-DAWN light-scattering detector ($\lambda = 690$ nm), a quasielastic light scattering detector, differential refractometry, and an absorption detector (280 nm). Molecular masses were calculated using Astra software (Wyatt Technologies) and the Debye fit method (30). A gel filtration marker kit (29–700-kDa range) from Sigma-Aldrich was used to confirm the accuracy of the measured masses.

AUC—Protein samples were first dialyzed against 100 mM NaCl, 25 mM Tris-HCl (pH 7.5) to remove glycerol and DTT. AUC was performed using a Beckman Optima XL-I (AN-60 Ti rotor) fitted with absorbance and interference optics. Epon double-sector centerpieces were filled with 400 μl of sample solution or blank buffer and sedimented at 29,160 × *g* for 24 h at 20 °C. Absorbance data were acquired at $\lambda = 280$ nm with time intervals of 2 min; interference scans were taken with time intervals of 1 min. Buffer viscosity, protein partial specific volumes, and frictional ratios were calculated using SEDNTERP (31). Data were analyzed using SEDFIT (32).

Enzyme kinetic measurements

Kinetic analyses of ICL were carried out using two types of assay. In the "direct assay," the enzyme was incubated in 25 mM imidazole, 5 mM $MgCl_2$, 1 mM EDTA, 4 mM phenylhydrazine (pH 6.8) with a range of substrate concentrations (0–600 μM). The resulting glyoxylate-phenylhydrazone ($\epsilon_{calc} = 16{,}800$ M^{-1} cm^{-1}) was measured spectrophotometrically at $\lambda = 324$ nm. In the "coupled assay," the enzyme was incubated in 50 mM MOPS-NaOH, 15 mM $MgCl_2$, 5 mM DTT, 1 mM EDTA (pH 7.3) containing 400 μM NAD^+ and 60 units of lactate dehydrogenase from pig heart. The reduction of NAD^+ to NADH ($\epsilon_{calc} =$ 6220 M^{-1} cm^{-1}) was measured spectrophotometrically at 340 nm. All assays were carried out at 37 °C.

The enzyme activity of IDH and ICD were measured using the same assay. The enzyme was incubated in 50 mM Tris-HCl, 5 mM $MgCl_2$ (pH 7.5). To measure the K_m value for isocitrate, initial rates were measured across a range of (+)-potassium D-*threo*-isocitrate concentrations (0–600 μM) with a fixed concentration of $NADP^+$ (200 μM). To measure the K_m value for $NADP^+$, initial rates were measured across a range of $NADP^+$ concentrations (0–600 μM) at a fixed concentration of isocitrate (200 μM). NADPH formation was recorded spectrophotometrically at $\lambda = 340$ nm ($\epsilon_{calc} = 6220$ M^{-1} cm^{-1}). All assays were carried out at 37 °C.

$AceK_{EC}$ and $AceK_{PA}$ kinase/phosphatase activity was assayed by coupling AceK activity to ICD activity as described previously (33) with the following modifications. In a 96-well plate, 180 μl of phosphorylation reaction mixture (100 mM Tris-HCl, 1 mM ATP, 2 mM $MgCl_2$, (pH 7.0) containing 10 μg of ICD and 5 μg of AceK) was incubated in each well for 1 h at 37 °C. Following this, putative allosteric regulators were added to each reaction mixture to a 5 mM final concentration. Each assay was carried out in triplicate. The reactions were then reincubated for a further 30 min at 37 °C to allow dephosphorylation of ICD and reactivation of ICD kinase activity. Aliquots (20 μl) of the reaction mixture were then transferred to a new UV-clear 96-well plate, and 180 μl of reduction solution consisting of 100 mM Tris-HCl, 1 mM *threo*-DL-isocitrate, 0.5 mM $NADP^+$, and 2 mM $MnCl_2$ (pH 7.0) was added to each well. The activity of ICD was detected spectrophotometrically by monitoring the rate of reduction of $NADP^+$ at 340 nm using a FLUOstar Omega plate reader (BMG Labtech). As a control, ICD alone was assayed for its ability to reduce $NADP^+$ in the presence of the putative allosteric regulators using the same method. Because phosphorylation of ICD by AceK inhibits the activity of ICD, higher ICD activity corresponds to increased AceK phosphatase activity. Confirmation of $AceK_{PA/EC}$ phosphotransfer to $ICD_{PA/EC}$ was also demonstrated using a ^{32}P-based phosphotransfer assay. The reaction conditions were identical to those described above; however, [γ-^{32}P]ATP (PerkinElmer Life Sciences) was used in place of unlabeled ATP. The proteins were resolved by SDS-PAGE, and radiolabeling was revealed using a phosphor screen (GE Healthcare). Radioactivity was determined with a Typhoon PhosphorImager and quantitated with ImageQuant.

Crystallization conditions

Crystallization conditions were screened and then optimized using sitting drop vapor diffusion with 18, 17.5, and 10 mg/ml of purified protein for ICL, IDH, and ICD, respectively. Crystals were obtained with a 1:1 protein/mother liquor mixture using a dragonfly® discovery system (TTP LabTech) for mother liquor preparation and a crystallization robot (mosquito® HTS, TTP LabTech) for liquid handling. ICL crystallized with 100 mM HEPES, 100 mM $CaCl_2$, 20% (w/v) PEG 6000, 5% (v/v) glycerol, 1 mM glyoxylate (pH 5.0), and 2% thymol as additive. IDH crystallized in the presence of 200 mM NaH_2PO_4, 21.5% (w/v) PEG 3350, 5% (v/v) glycerol, and 150 μM $NADP^+$. ICD crystallized in 100 mM sodium acetate, 30% (v/v) PEG 300 (pH 4.6). All crystals were grown for 2–6 days at 19 °C and then treated with cryoprotectant (24% (v/v) ethylene glycol and 76% (v/v) mother solution) before mounting in loops for data collection.

X-ray diffraction, structure determination, and refinement

Diffraction data were collected remotely on the I02 or I04-1 beamline (as indicated in Table S1) at the Diamond Light Source Synchrotron (Didcot, UK). Diffraction data were processed using FastDP (33), and the structures were determined by molecular replacement using Phaser (34). ICL, IDH, and ICD were solved using the structural templates 3I4E (to be published), 4ZDA (to be published), and 1BL5 (35) from *Burkholderia pseudomallei*, *M. smegmatis*, and *E. coli*, respectively. Automated refinement was performed using Refmac5 (36). Manual modeling and refinement were performed in COOT (36). Data collection and refinement statistics are listed in Table S1.

Western blotting

Polyclonal antibodies were raised in rabbits against each of the purified proteins (BioGenes GmbH). The antisera were preabsorbed against an acetone extract of a mutant strain defective in the protein of interest (*e.g.* the anti-ICD antisera were preabsorbed against an acetone extract of a confirmed *icd* mutant). The cleaned-up antisera, appropriately diluted, were then used directly in Western assays. Western blots were developed using goat anti-rabbit secondary antibodies.

Author contributions—A. C. data curation; A. C., S. K. D., P. B., D. Y. C., and M. W. formal analysis; A. C., S. K. D., P. B., and D. Y. C. investigation; A. C. and S. K. D. methodology; A. C. and M. W. writing-original draft; A. C., S. K. D., P. B., D. Y. C., and M. W. writing-review and editing; M. W. conceptualization; M. W. supervision; M. W. funding acquisition; M. W. project administration.

References

1. Kornberg, H. L. (1966) The role and control of the glyoxylate cycle in *Escherichia coli*. *Biochem. J.* **99,** 1–11 CrossRef Medline
2. LaPorte, D. C., Walsh, K., and Koshland, D. E., Jr. (1984) The branch point effect ultrasensitivity and subsensitivity to metabolic control. *J. Biol. Chem.* **259,** 14068–14075 Medline

3. Walsh, K., and Koshland, D. E. (1984) Determination of flux through the branch point of two metabolic cycles: the tricarboxylic acid cycle and the glyoxylate shunt. *J. Biol. Chem.* **259,** 9646–9654 Medline
4. Walsh, K., and Koshland, D. E. (1985) Branch point control by the phosphorylation state of isocitrate dehydrogenase: a quantitative examination of fluxes during a regulatory transition. *J. Biol. Chem.* **260,** 8430–8437 Medline
5. Dean, A. M., Lee, M. H. I., and Koshland, D. E., Jr. (1989) Phosphorylation inactivates *Escherichia coli* isocitrate dehydrogenase by preventing isocitrate binding. *J. Biol. Chem.* **264,** 20482–20486 Medline
6. Nimmo, G. A., and Nimmo, H. G. (1984) The regulatory properties of isocitrate dehydrogenase kinase and isocitrate dehydrogenase phosphatase from *Escherichia coli* ML308 and the roles of these activities in the control of isocitrate dehydrogenase. *Eur. J. Biochem.* **141,** 409–414 CrossRef Medline
7. Murima, P., Zimmermann, M., Chopra, T., Pojer, F., Fonti, G., Dal Peraro, M., Alonso, S., Sauer, U., Pethe, K., and McKinney, J. D. (2016) A rheostat mechanism governs the bifurcation of carbon flux in mycobacteria. *Nat. Commun.* **7,** 12527 CrossRef Medline
8. Kornberg, H. L., and Madsen, N. B. (1957) Synthesis of C4-dicarboxylic acids from acetate by a "glyoxylate bypass" of the tricarboxylic acid cycle. *Biochim. Biophys. Acta.* **24,** 651–653 CrossRef Medline
9. Berger, A., Dohnt, K., Tielen, P., Jahn, D., Becker, J., and Wittmann, C. (2014) Robustness and plasticity of metabolic pathway flux among uropathogenic isolates of *Pseudomonas aeruginosa*. *PLoS One* **9,** e88368 CrossRef Medline
10. Díaz-Pérez, A. L., Román-Doval, C., Díaz-Pérez, C., Cervantes, C., Sosa-Aguirre, C. R., López-Meza, J. E., and Campos-García, J. (2007) Identification of the *aceA* gene encoding isocitrate lyase required for the growth of *Pseudomonas aeruginosa* on acetate, acyclic terpenes and leucine. *FEMS Microbiol. Lett.* **269,** 309–316 CrossRef Medline
11. Britton, K., Langridge, S., Baker, P. J., Weeradechapon, K., Sedelnikova, S. E., De Lucas, J. R., Rice, D. W., and Turner, G. (2000) The crystal structure and active site location of isocitrate lyase from the fungus *Aspergillus nidulans*. *Structure* **8,** 349–362 Medline
12. Britton, K. L., Abeysinghe, I. S. B., Baker, P. J., Barynin, V., Diehl, P., Langridge, S. J., McFadden, B. A., Sedelnikova, S. E., Stillman, T. J., Weeradichapon, K., and Rice, D. W. (2001) The structure and domain organization of *Escherichia coli* isocitrate lyase. *Acta Crystallogr. D Biol. Crystallogr.* **57,** 1209–1218 CrossRef Medline
13. Sharma, V., Sharma, S., Hoener zu Bentrup, K., McKinney, J. D., Russell, D. G., Jacobs, W. R., Jr., and Sacchettini, J. C. (2000) Structure of isocitrate lyase, a persistence factor of *Mycobacterium tuberculosis*. *Nat. Struct. Biol.* **7,** 663–668 CrossRef Medline
14. Rittenhouse, J. W., and McFadden, B. A. (1974) Inhibition of isocitrate lyase from *Pseudomonas indigofera* by itaconate. *Arch. Biochem. Biophys.* **163,** 79–86 CrossRef Medline
15. Schloss, J. V., and Cleland, W. W. (1982) Inhibition of isocitrate lyase by 3-nitropropionate, a reaction-intermediate analogue. *Biochemistry* **21,** 4420–4427 CrossRef Medline
16. Krissinel, E., and Henrick, K. (2007) Inference of macromolecular assemblies from crystalline state. *J. Mol. Biol.* **372,** 774–797 CrossRef Medline
17. Yasutake, Y., Watanabe, S., Yao, M., Takada, Y., Fukunaga, N., and Tanaka, I. (2002) Structure of the monomeric isocitrate dehydrogenase: evidence of a protein monomerization by a domain duplication. *Structure* **10,** 1637–1648 CrossRef Medline
18. Nimmo, H. G. (1986) Kinetic mechanism of *Escherichia coli* isocitrate dehydrogenase and its inhibition by glyoxylate and oxaloacetate. *Biochem. J.* **234,** 317–323 CrossRef Medline
19. Hurley, J. H., Thorsness, P. E., Ramalingam, V., Helmers, N. H., Koshland, D. E., Jr., and Stroud, R. M. (1989) Structure of a bacterial enzyme regulated by phosphorylation, isocitrate dehydrogenase. *Proc. Natl. Acad. Sci. U.S.A.* **86,** 8635–8639 CrossRef Medline
20. Son, M. S., Matthews, W. J., Jr., Kang, Y., Nguyen, D. T., and Hoang, T. T. (2007) *In vivo* evidence of *Pseudomonas aeruginosa* nutrient acquisition and pathogenesis in the lungs of cystic fibrosis patients. *Infect. Immunity* **75,** 5313–5324 CrossRef Medline
21. McVey, A. C., Medarametla, P., Chee, X., Bartlett, S., Poso, A., Spring, D. R., Rahman, T., and Welch, M. (2017) Structural and functional characterization of malate synthase G from opportunistic pathogen *Pseudomonas aeruginosa*. *Biochemistry* **56,** 5539–5549 CrossRef Medline
22. Fahnoe, K. C., Flanagan, M. E., Gibson, G., Shanmugasundaram, V., Che, Y., and Tomaras, A. P. (2012) Non-traditional antibacterial screening approaches for the identification of novel inhibitors of the glyoxylate shunt in Gram-negative pathogens. *PLoS One* **7,** e51732 CrossRef Medline
23. Chung, J. C. S., Rzhepishevska, O., Ramstedt, M., and Welch, M. (2013) Type III secretion system expression in oxygen-limited *Pseudomonas aeruginosa* cultures is stimulated by isocitrate lyase activity. *Open Biol.* **3,** 120131 CrossRef Medline
24. Lindsey, T. L., Hagins, J. M., Sokol, P. A., and Silo-Suh, L. A. (2008) Virulence determinants from a cystic fibrosis isolate of *Pseudomonas aeruginosa* include isocitrate lyase. *Microbiology* **154,** 1616–1627 CrossRef Medline
25. McKinney, J. D., Höner zu Bentrup, K., Muñoz-Elías, E. J., Miczak, A., Chen, B., Chan, W. T., Swenson, D., Sacchettini, J. C., Jacobs, W. R., Jr., and Russell, D. G. (2000) Persistence of *Mycobacterium tuberculosis* in macrophages and mice requires the glyoxylate shunt enzyme isocitrate lyase. *Nature* **406,** 735–738 CrossRef Medline
26. Singh, R., Mailloux, R. J., Puiseux-Dao, S., and Appanna, V. D. (2007) Oxidative stress evokes a metabolic adaptation that favors increased NADPH synthesis and decreased NADH production in *Pseudomonas fluorescens*. *J. Bacteriol.* **189,** 6665–6675 CrossRef Medline
27. Lassek, C., Berger, A., Zühlke, D., Wittmann, C., and Riedel, K. (2016) Proteome and carbon flux analysis of *Pseudomonas aeruginosa* clinical isolates from different infection sites. *Proteomics* **16,** 1381–1385 CrossRef Medline
28. Dunn, M. F., Ramírez-Trujillo, J. A., and Hernández-Lucas, I. (2009) Major roles of isocitrate lyase and malate synthase in bacterial and fungal pathogenesis. *Microbiology* **155,** 3166–3175 CrossRef Medline
29. Zheng, J., Lee, D. C., and Jia, Z. (2009) Purification, crystallization and preliminary X-ray analysis of isocitrate dehydrogenase kinase/phosphatase from *Escherichia coli*. *Acta Crystallogr. Sect. F Struct. Biol. Cryst. Commun.* **65,** 536–539 CrossRef Medline
30. Wyatt, P. J. (1993) Light scattering and the absolute characterization of macromolecules. *Anal. Chim. Acta* **272,** 1–40 CrossRef
31. Hayes, D., Laue, T., and Philo, J. (1995) SEDNTERP, University of New Hampshire, Durham, NH
32. Zhao, H., Brautigam, C. A., Ghirlando, R., and Schuck, P. (2013) Current methods in sedimentation velocity and sedimentation equilibrium analytical ultracentrifugation. *Curr. Protoc. Protein Sci.*, Chapter 20, Unit 20.12 CrossRef Medline
33. Winter, G., and McAuley, K. E. (2011) Automated data collection for macromolecular crystallography. *Methods* **55,** 81–93 CrossRef Medline
34. McCoy, A. J., Grosse-Kunstleve, R. W., Adams, P. D., Winn, M. D., Storoni, L. C., and Read, R. J. (2007) Phaser crystallographic software. *J. Appl. Crystallogr.* **40,** 658–674 CrossRef Medline
35. Stoddard, B. L., Cohen, B. E., Brubaker, M., Mesecar, A. D., and Koshland, D. E. (1998) Millisecond Laue structures of an enzyme-product complex using photocaged substrate analogs. *Nat. Struct. Biol.* **5,** 891–897 CrossRef Medline
36. Emsley, P., and Cowtan, K. (2004) Coot: model-building tools for molecular graphics. *Acta Crystallogr. D Biol. Crystallogr.* **60,** 2126–2132 CrossRef Medline